Superiority of TiO_2 Supported on the Nickel Foam Over Ni Doped TiO_2 in the Photothermal Decomposition of Acetaldehyde

Beata Tryba *, Piotr Miądlicki, Piotr Rychtowski, Maciej Trzeciak, Rafał Jan Wróbel

Posted Date: 26 June 2023

doi: 10.20944/preprints202306.1825.v1

Keywords: thermo-photocatalysis; nickel foam; Ni doped TiO2; acetaldehyde decomposition

Article

Superiority of TiO_2 supported on the nickel foam over Ni doped TiO_2 in the photothermal decomposition of acetaldehyde

Beata Tryba*, Piotr Miądlicki, Piotr Rychtowski, Maciej Trzeciak and Rafał Wróbel

West Pomeranian University of Technology in Szczecin, Faculty of Chemical Technology and Engineering, Engineering of Catalytic and Sorbent Materials Department, Pułaskiego 10, PL 70-322 Szczecin, Poland.

* Correspondence: author's e-mail address: beata.tryba@zut.edu.pl

Abstract: Acetaldehyde decomposition was performed under heating at the temperature range of 25-125°C and UV irradiation on TiO_2 doped by the metallic Ni powder and TiO_2 supported on the nickel foam. Process was carried out in high temperature reaction chamber "The Praying Mantis™", with simultaneous *in situ* FTIR measurements and UV irradiation. Ni powder was added to TiO_2 in the quantity of 0.5 to 5.0 wt%. Photothermal measurements of acetaldehyde decomposition indicated, that the highest yield of acetaldehyde conversion on TiO_2 und UV irradiation was obtained at 75°C. Doping of nickel to TiO_2 did not increase its photocatalytic activity. Contrary to that, application of nickel foam as a support for TiO_2 appeared to be highly advantageous, because increased decomposition of acetaldehyde from 31 to 52% at 25°C and then to 85% at 100°C by comparison with TiO_2 itself. At the same time mineralisation of acetaldehyde to CO_2 increased two times at the presence of nickel foam. However, oxidised nickel foam used as support for TiO_2 was detrimental. Most likely, different mechanisms of electrons transfer between Ni-TiO_2 and NiO-TiO_2 occurred. Application of nickel foam greatly enhanced separation of free carriers in TiO_2. As a consequence, high yields of the photocatalytic reactions were obtained.

Keywords: thermo-photocatalysis; nickel foam; Ni doped TiO_2; acetaldehyde decomposition

1. Introduction

Photo-thermal catalysis combines photo-chemical and thermochemical contributions of sunlight and has emerged as a rapidly growing and exciting new field of research [1–3].

Photo-thermal catalysis with application of semiconductor doped by metallic nanoparticles allows for a more effective harvesting of the solar spectrum, including low-energy visible and infrared photons.

Certain metallic nanoparticles (NPs) such as Au, Ag, Cu and others exhibit unique optical properties related to the localized surface plasmon resonance (LSPR), which can be tunable by varying their size and shape across the entire visible spectrum [4,5].

In the LSPR process hot charge carriers are generated, which possess higher energies than those induced by direct photoexcitation. These energetic carriers can be transferred to the adsorbate surface or conductive band of semiconductor or can relax internally and dissipate their energy by local heating of the surroundings, causing a thermal effect on the material. This photo-thermal effect has been extensively applied in a large number of fields, including cancer therapy, degradation of pollutants, CO_2 reduction, hydrogen production by water splitting and other chemical reactions such as ex. catalytic steam reforming or hydrogenation of olefins [2,6–13]. Photo-thermal effect can be also obtained in non-plasmonic structures through direct intraband and/or interband electronic transitions. For instance, Sarina et al. [14] demonstrated that non-plasmonic metal NPs supported on ZrO_2 could

 doi:10.20944/preprints202306.1825.v1

catalyze cross-coupling reactions at low temperatures under visible light. According to the authors, upon irradiation with UV light electrons could shift to high-energy levels through interband transitions, and only those with enough energy could transfer to the LUMO of adsorbed molecules, just like in the case of plasmonic metal NPs. When excited with low-energy visible-IR light, electrons were not energetic enough to be injected into adsorbate states, thus contributing to the enhancement of the reaction rate by means of thermal effects. Altogether, photochemical and thermal effects contribute to the photo-thermal performance in non-plasmonic semiconductors.

The size, shape and quantity of the plasmonic nanoparticles contributing in the photo-thermal effect are important. The temperature increase is proportional to the square of the nanoparticle radius. However, it was theorized, that the temperature increment due to the irradiation of a single nanoparticle became negligible, but the light-induced heating effect could be strongly enhanced in the presence of a large number of NPs owing to the collective effects [2]. Theoretical calculations have demonstrated that larger plasmonic NPs provide a larger amount of hot carriers, but they display energies close to the Fermi level, since most of the absorbed energy is dissipated either by scattering or by heating. In contrast, smaller NPs exhibit higher energies but they are showing very short lifetimes [2]. Lower size plasmonic NPs show blue shift absorption edge due to the quantum size effect [15]. All these parameters are extremely important during design the nanomaterial for the thermo-photocatalytic processes.

The most intensively explored plasmonic NPs used in the photo-thermal processes so far are based on Au, Ag, Pd, Cu and Pt nanoparticles, less are reported on the other metals such as Ni or Co. Thermo-photocatalytic decomposition of acetaldehyde was reported on TiO_2 doped by Pt, Ag, Pd, or Au nanoparticles [10,16–19]. Among all these doped metals to TiO_2, Pt had the highest activity due to the strong thermo-catalytic effect at elevated temperature. The activity of metal or metal oxide doped to TiO_2 depended on the oxidation state of metal and their adsorption abilities towards acetaldehyde species. The other structures, such as metal nanowires coated by TiO_2 were also prepared and tested for the acetaldehyde removal [20,21]. There are some reports on application of nickel foam with loaded TiO_2 for different purposes, such as: anode for lithium-ion batteries [22], hydrogen evolution from water splitting [23], toluene and acetaldehyde decompositions [24,25], nitrogen oxides removal [26] and others. Nickel foam was also used as a support and catalyst for different materials in the photocatalytic processes [27–29]. As a main advantage of application the nickel foam as a composite with other photocatalyst is significant improvement of charge separation in the photocatalytic material.

Although some reports on the application of nickel foam with loaded TiO_2 have been already published, in these studies there is proposed the first time mechanism of thermo-photocatalytic decomposition of acetaldehyde under UV light at the presence of TiO_2 supported on the nickel foam, and this is compared with others, which occur, when oxidised nickel foam or nanosized Ni particles added to TiO_2 are utilised.

2. Materials and Methods

TiO_2 of anatase phase was obtained by two-step process: hydrothermal treatment of amorphous titania (Police Chemical Factory, Poland) in deionized water in 150°C under pressure of 7.4 bar for 1 hour and following annealing in a pipe furnace in 400°C under Ar flow for 2 hours. Our previous work presented the detailed physicochemical characterizations of this material [30].

Nickel foam (China) with purity of 99.8% had the following parameters: thickness: 1.5mm, porosity: 95%-97%, Surface density: 300 g/m^2. Nickel powder (Warchem, Poland) had a purity of 99.8%.

XRD measurements of nickel foams were performed using the diffractometer (PANanalytical, The Netherlands) with a Cu X-ray source, λ = 0.154439 nm. Measurements were conducted in the 2θ range of 10-100° with a step size of 0.013. The applied voltage was 35 kV and the current was 30 mA.

SEM/EDS images were obtained using a field emission scanning electron microscope with high resolution (UHR FE-SEM, Hitachi, Japan).

Preprints (www.preprints.org) | NOT PEER-REVIEWED | Posted: 26 June 2023 doi:10.20944/preprints202306.1825.v1

Oxidation of nickel foams was carried out in a muffle furnace (Czylok SM-2002, Poland) at 500°C for 1 hour.

The chemical composition was determined through X-ray photoelectron spectroscopy (XPS) analysis. The measurements were conducted using a commercial multipurpose ultra-high vacuum (UHV) surface analysis system (PREVAC, Rogow, Poland). A nonmonochromatic XPS source and a kinetic electron energy analyzer (SES 2002; Scienta) was used. The spectrometer was calibrated using the Ag 3d5/2 transition. The XPS analysis utilized Mg Kα (h=1253.6 eV) radiation as the excitation source.

The size of nickel powdered nanoparticles was determined using an atomic force microscope (AFM; NanoScope V Multimode 8, Bruker, USA) with a silicon nitride probe in ScanAsyst mode. Prior to measurement, the samples were dispersed in isopropyl alcohol and then drop casted onto a silicon wafer. Obtained surface topography images were obtained using NanoScope Analysis software, whereas particle sizes were evaluated via ImageJ software.

Thermo-photocatalytic decomposition tests of acetaldehyde were conducted using high temperature reaction chamber (Harrick, USA), as shown in Fig 1. During the test, continuous FTIR measurements were conducted using Thermo Nicolet iS50 FTIR instrument (Thermo, USA).

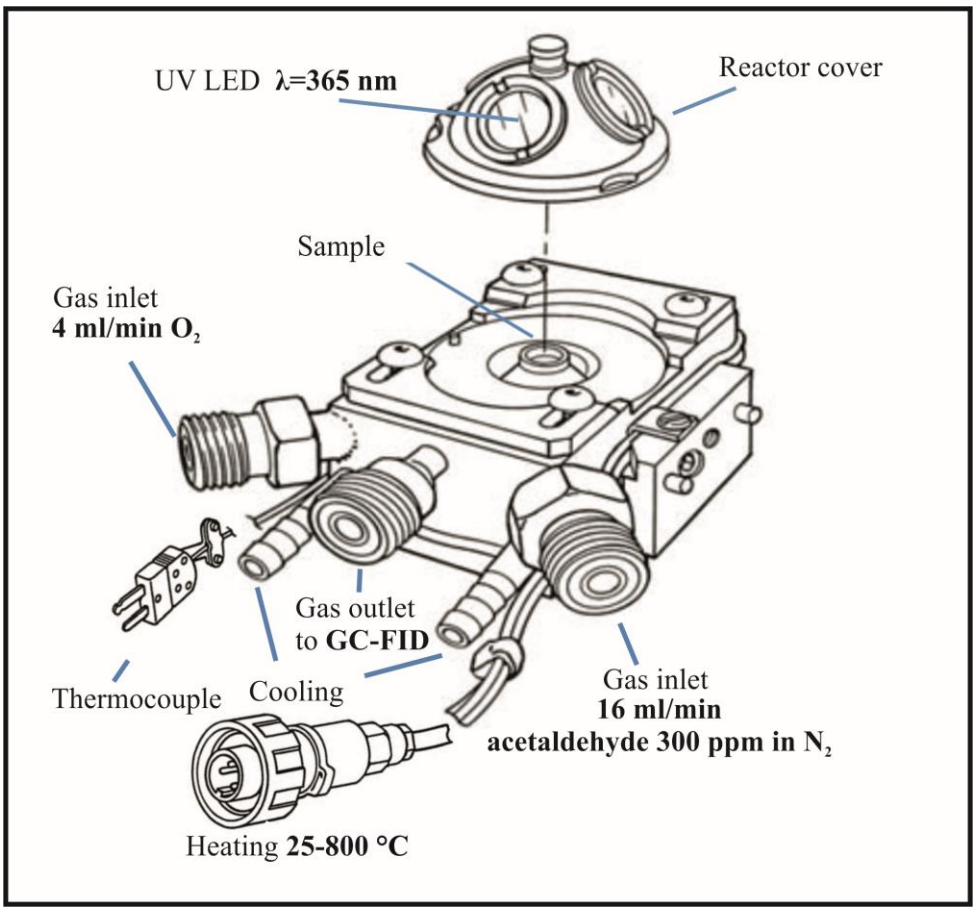

Figure 1. The scheme of The Praying Mantis™ High Temperature Reaction Chamber.

UV irradiation was conducted through a quartz window, with an illuminator equipped with a fiber optics and a UV-LED, 365 nm diode with an optical power of 415 mW (Poland, LABIS). Gases were supplied from bottles through two inlets using mass flow meters. The first one was acetaldehyde in nitrogen, 300 ppm (Messer), the second one was a synthetic oxygen with purity 5.0 (Messer). Gases have been mixed in proportions to create a synthetic air composition. After the thermo-photocatalytic process the gas stream was directed to the gas chromatograph (GC) equipped with automatically dosing sample loop (GC-FID, SRI, USA). Acetaldehyde concentration was determined from

Preprints (www.preprints.org) | NOT PEER-REVIEWED | Posted: 26 June 2023 doi:10.20944/preprints202306.1825.v1

recorded chromatograms in GC. Outlet gas stream from GC was flowing through the CO_2 sensor (APFinder CO_2, ATUT Company, Poland) in order to monitor the quantity of CO_2 formed upon acetaldehyde mineralization.

The catalytic systems that have been used in the tests are as follows: a) TiO_2, b) a thin layer (1mm) of TiO_2 supported on KBr which is inert to acetaldehyde, c) a thin layer of TiO_2 supported on Ni foam, d) a thin layer of TiO_2 supported on the oxidised Ni foam, e) TiO_2 blended with the nickel powder in the various amount, 0.5-5 wt. %. In Fig. 2 there is illustrated the scheme of the materials compositions used for the photocatalytic tests of acetaldehyde decomposition.

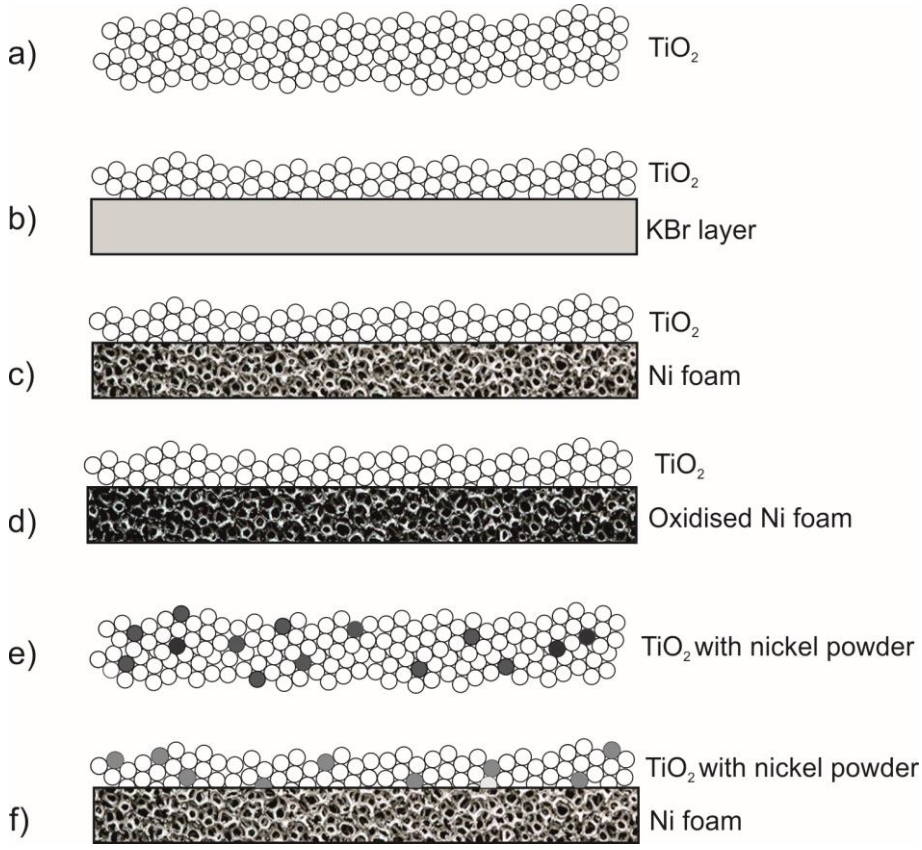

Figure 2. Catalytic systems used during thermo-photocatalytic decomposition of acetaldehyde.

3. Results

The results from the thermo-photocatalytic decomposition of acetaldehyde over TiO_2 and UV LED irradiation are illustrated in Fig. 3.

Preprints (www.preprints.org) | NOT PEER-REVIEWED | Posted: 26 June 2023 doi:10.20944/preprints202306.1825.v1

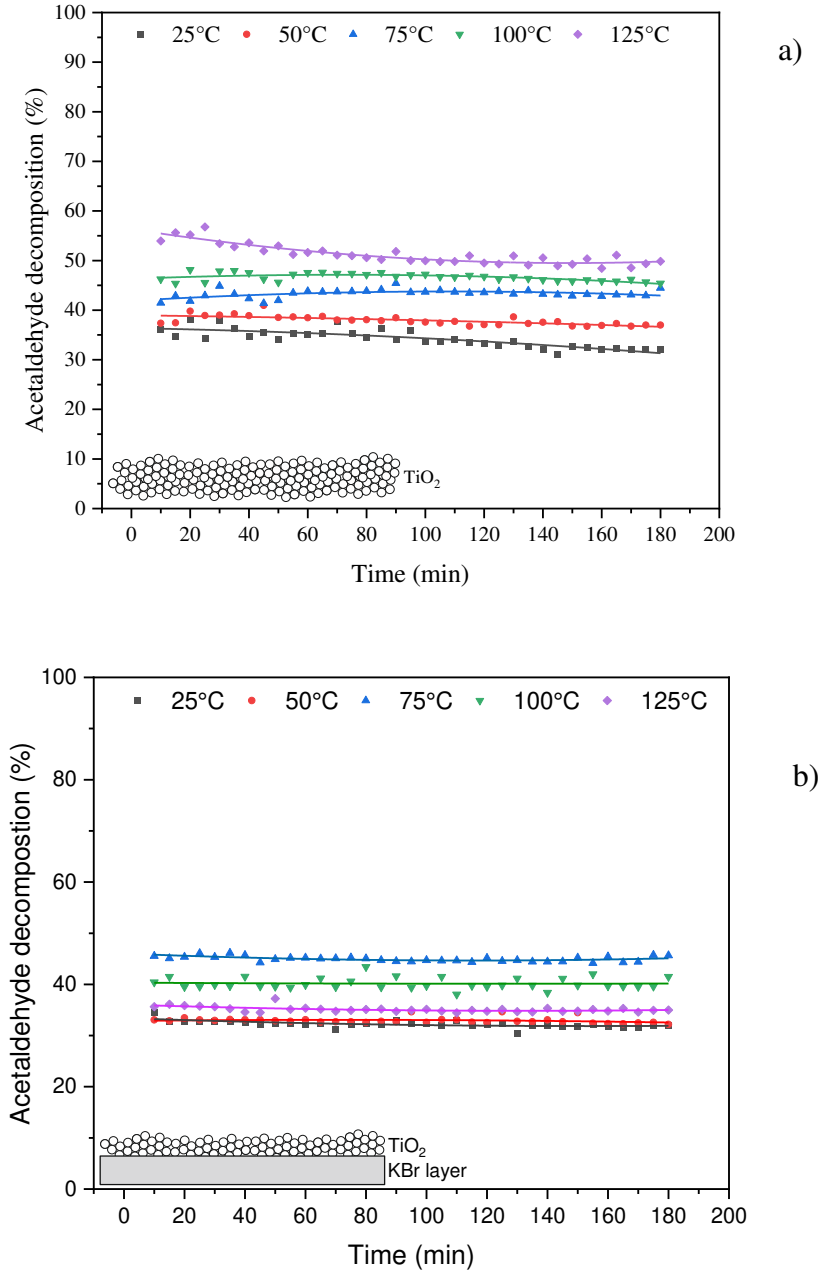

Figure 3. Photocatalytic decomposition of acetaldehyde under UV irradiation at various reaction temperatures at the presence of: a) TiO_2, b) TiO_2 supported on KBr.

Performed measurements indicated, that conversion of acetaldehyde on TiO_2 could be enhanced at elevated temperature, In case of a thick layer of TiO_2 used (without KBr), Fig. 3b, the highest acetaldehyde conversion was observed at 125°C, however this process was not stable and indicated gradual falling-off in degradation rate, reaching its maximum after 180 min of UV irradiation with conversion of 50%. Contrary to that, application of a thin layer TiO_2 supported on KBr allowed to get stabilization of the process, but the highest conversion of acetaldehyde was lower than in case of using TiO_2 only and reached 47% at 75°C. In Table 1 there are presented results from measurements of CO_2 in the outlet stream of reacted gases.

 doi:10.20944/preprints202306.1825.v1

Table 1. Content of CO_2 in a gas stream after acetaldehyde decomposition on TiO_2.

Reaction temperature (°C)	CO_2 (ppm)	
	TiO_2	TiO_2 on KBr
25	220	245
50	235	245
75	232	300
100	210	330
125	225	290

These results indicated, that mineralization of acetaldehyde was higher in case of the photocatalytic system used with a thin layer of TiO_2. Acetaldehyde can be oxidized over TiO_2 in a dark at the presence of oxygen, however its complete mineralization occurs at the presence of reactive radicals. Most likely TiO_2 at the bottom of reactor chamber was not activated by UV light, and formed products of acetaldehyde decomposition at the lower part of TiO_2 were scavengers for reactive radicals formed at the surface of TiO_2 on the top of reactor. Therefore, for higher quantity of TiO_2 used, acetaldehyde conversion was higher, but its mineralization to CO_2 dropped down.

In Fig. 4 there are presented results from the thermo-photocatalytic decomposition of acetaldehyde over TiO_2 supported on the nickel foam.

Preprints (www.preprints.org) | NOT PEER-REVIEWED | Posted: 26 June 2023 doi:10.20944/preprints202306.1825.v1

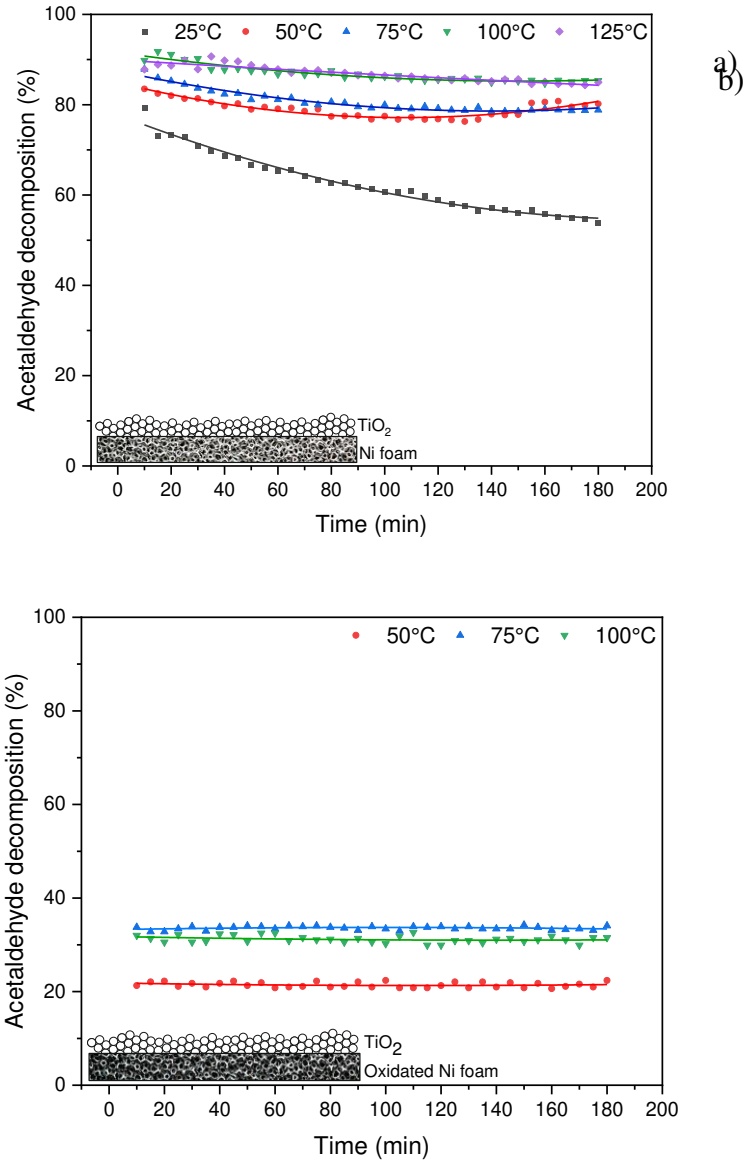

Figure 4. Photocatalytic decomposition of acetaldehyde under UV irradiation at various reaction temperatures at the presence of: a) TiO_2 supported on Ni foam, b) TiO_2 supported on oxidized Ni foam.

High decomposition of acetaldehyde (around 85%) was observed at the presence of TiO_2 supported on Ni foam and reaction temperature of 100-125°C. The slight decrease in acetaldehyde decomposition over time is due to by-products blocking the catalyst's active centers. However the efficiency of this process significantly decreased at the presence of oxidised Ni foam, the decomposition of acetaldehyde dropped down to 33%. It has to be mentioned, that Ni foam as received was much less active than that after photocatalytic process. Therefore all the results presented in Fig. 4a were performed for reused nickel foam.

In Table 2 there are presented results from measurements of CO_2 after thermo-photocatalytic process of acetaldehyde decomposition conducted for TiO_2 supported on reused Ni foam and that oxidized at 500°C.

Table 2. Content of CO_2 in a gas stream after acetaldehyde decomposition on TiO_2.

Preprints (www.preprints.org) | NOT PEER-REVIEWED | Posted: 26 June 2023 doi:10.20944/preprints202306.1825.v1

Reaction temperature (°C)	CO_2 (ppm)	
	TiO_2 on reused Ni foam	TiO_2 on Ni foam oxidised at 500°C
25	364	-
50	409	<100
75	438	<100
100	472	<100
125	423	-

Application of reused Ni foam with TiO_2 not only enhanced decomposition rate of acetaldehyde, but also double increased its mineralization degree.

In Fig. 5 there are presented results from the photocatalytic decomposition of acetaldehyde over TiO_2 blended with nanosized Ni powder.

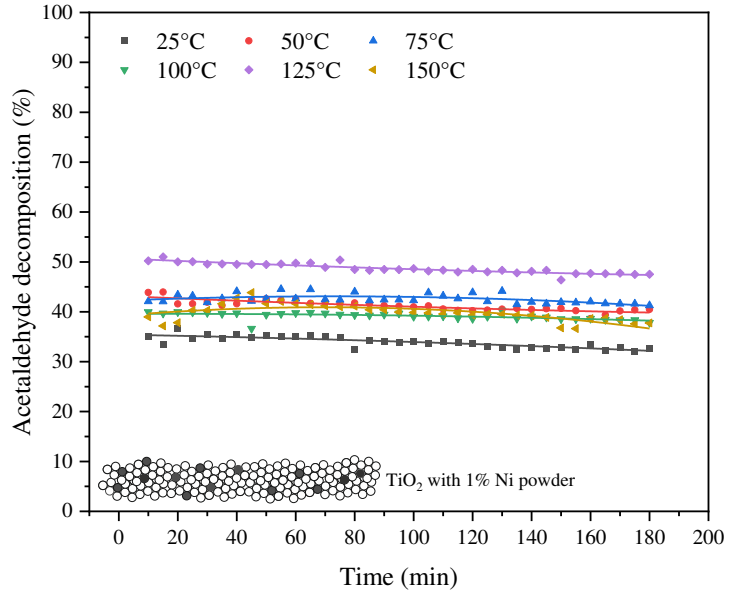

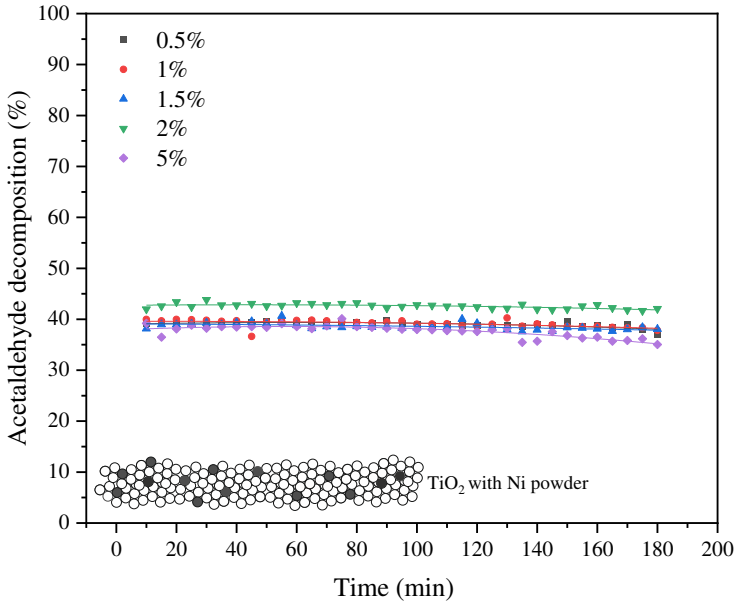

Preprints (www.preprints.org) | NOT PEER-REVIEWED | Posted: 26 June 2023 doi:10.20944/preprints202306.1825.v1

Figure 5. Photocatalytic decomposition of acetaldehyde under UV irradiation at the presence of TiO_2 with doped Ni powder; a) in various reaction temperatures and 1% of doped Ni, and b) for different quantity of doped Ni in reaction temperature of 100°C.

The quantity of doped Ni slightly affected the efficiency of acetaldehyde decomposition, which ranged from 38 to 43%. In temperature of 125°C the process yield was the highest and reached around 50% for 1% of doped Ni to TiO_2. Although acetaldehyde decomposition rate on TiO_2 doped with Ni was quite comparable with that for TiO_2, the mineralization degree was low, the maximum value of formed CO_2 was 150 ppm, which was reached for 1% of doped Ni at reaction temperature of 75°C, for the other tests the quantity of formed CO_2 was lower.

AFM analyses of surface topography with loaded Ni particles indicated, that their mean size was c.a. 30 nm, as shown in Fig. 6.

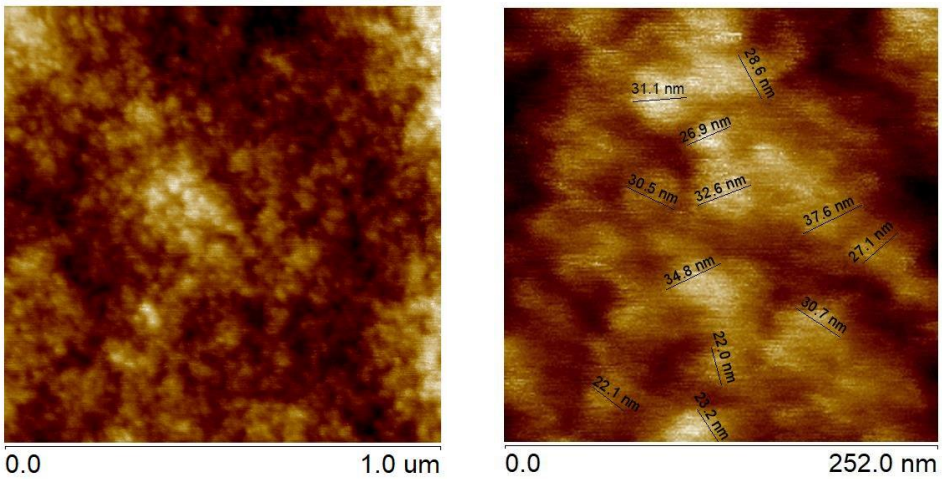

Figure 6. Surface topography of nickel nanoparticles.

In Fig. 7 XRD patterns of Ni foam as received and after oxidation at 500°C in air are illustrated.

Preprints (www.preprints.org) | NOT PEER-REVIEWED | Posted: 26 June 2023 doi:10.20944/preprints202306.1825.v1

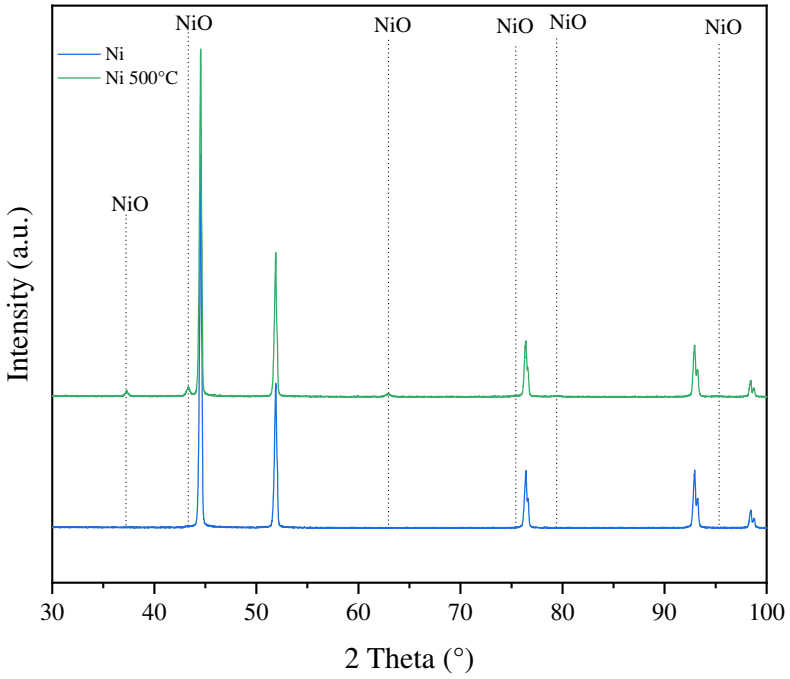

Figure 7. XRD patterns of Ni foam before and after oxidation at 500°C in air.

After oxidation of Ni foam in temperature of 500°C new reflexes emerged, which were ascribed to NiO phase, however their intensities were much lower than those related to Ni.

In Fig. 8 the SEM images of nickel foam are showed at different magnifications.

Preprints (www.preprints.org) | NOT PEER-REVIEWED | Posted: 26 June 2023 doi:10.20944/preprints202306.1825.v1

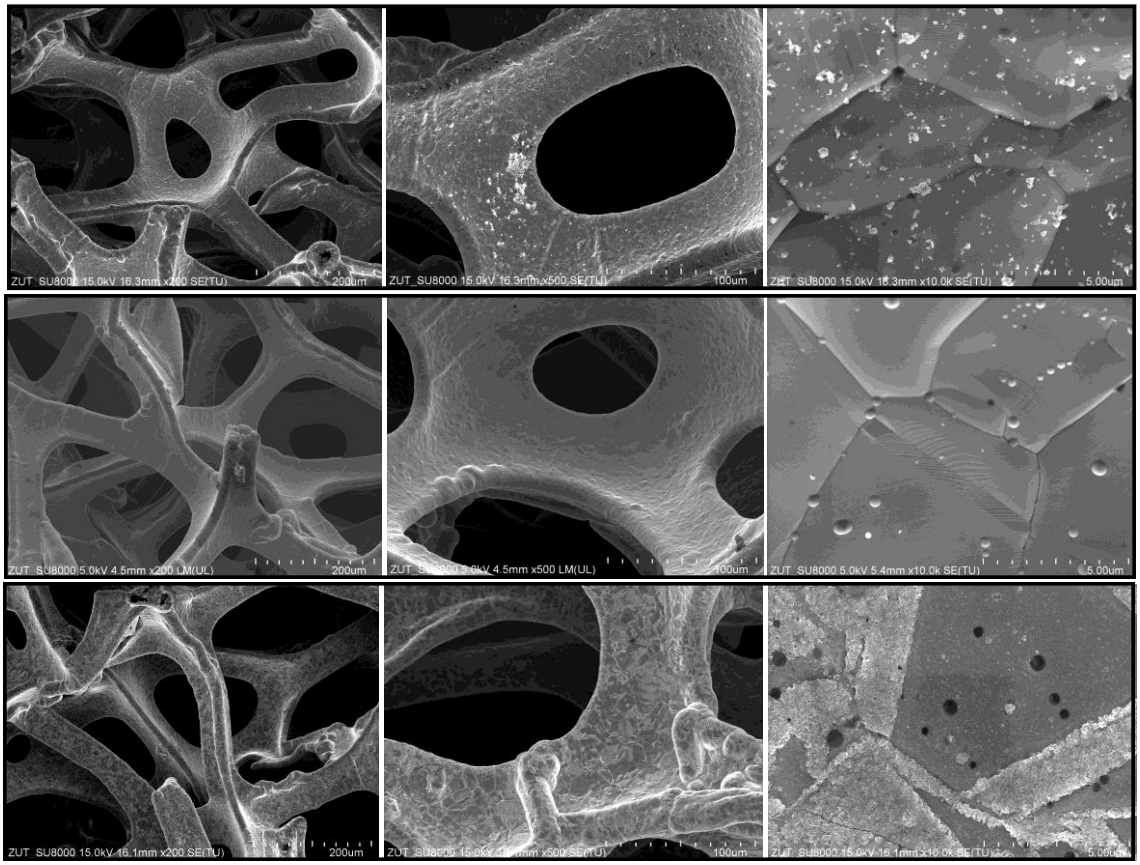

Figure 8. SEM images of a nickel foam, a) as received, b) after photocatalytic process and c) oxidized at 500°C in air.

Performed SEM images showed some impurities on the surface of nickel foam, as received from the manufacturer (Fig. 8a). After photocatalytic process these impurities disappeared (Fig. 8b). The oxidized nickel foam showed corrugated surface on the grain fringes, indicating on the proceeding oxidation process.

In Fig. 9 mapping of the oxidized nickel foam was depicted. The green area indicates an oxygen distribution. It is clearly seen, that strongly corrugated surface covers with elemental oxygen.

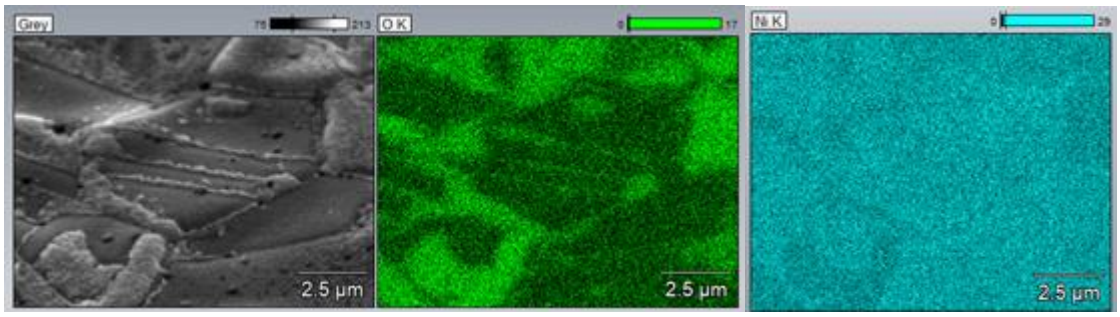

Figure 9. Elemental mapping of nickel foam surface oxidized at 500°C in air.

In the next step XPS analyses were performed for nickel foam as received (fresh), after photocatalytic process and that oxidized at 500°C in air. Recorded XPS spectra for C1s, Ni2p$_{3/2}$ and O1s signals are presented in Fig. 10.

Preprints (www.preprints.org) | NOT PEER-REVIEWED | Posted: 26 June 2023 doi:10.20944/preprints202306.1825.v1

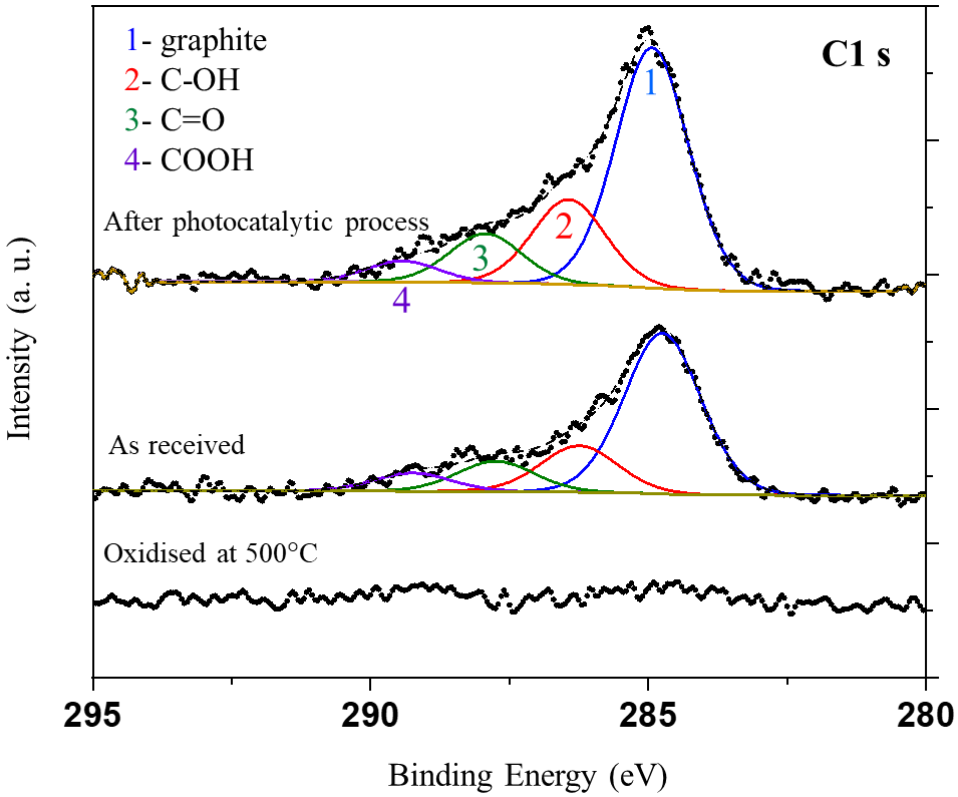

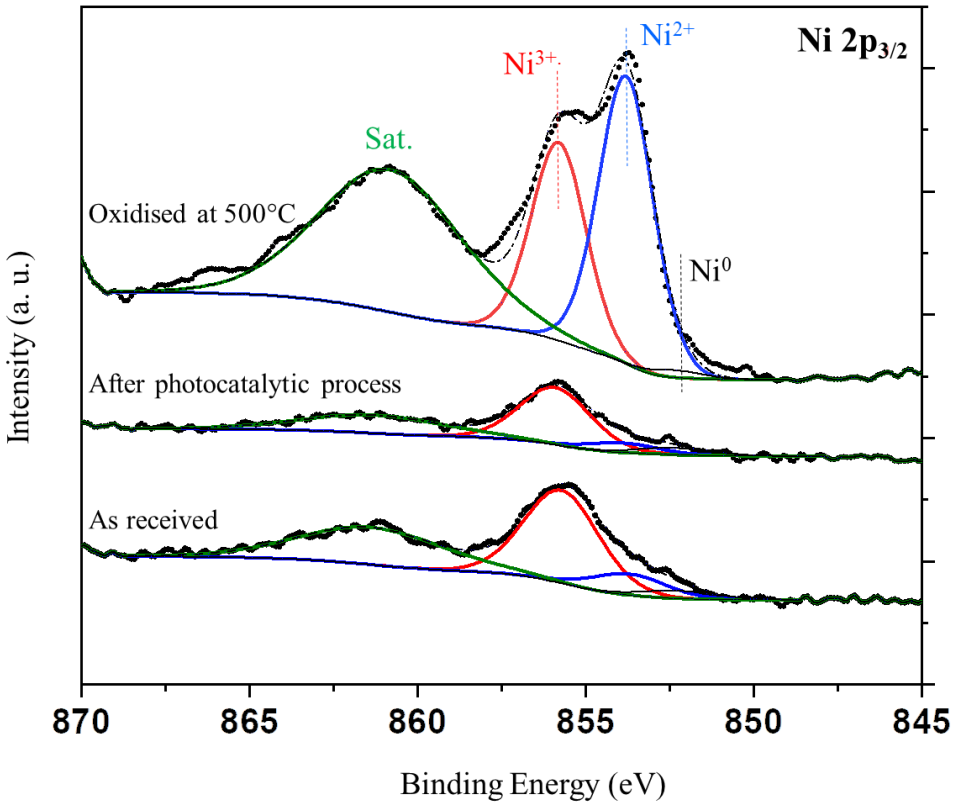

Preprints (www.preprints.org) | NOT PEER-REVIEWED | Posted: 26 June 2023 doi:10.20944/preprints202306.1825.v1

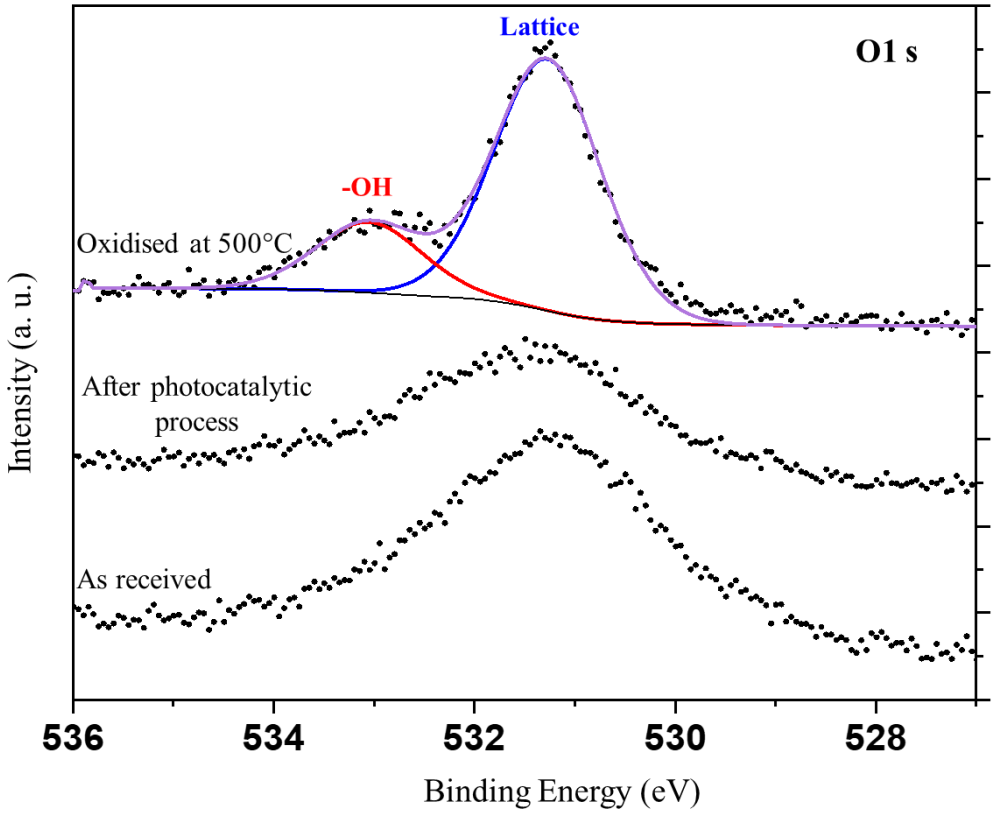

Figure 10. XPS spectra of nickel foams for C1s, Ni2p$_{3/2}$ and O1s signals.

The elemental surface content from XPS analyses is presented in Table 3.

Table 3. Elemental analyses of nickel foam surface.

Nickel foam	Elemental surface content (% at.)		
	O1s	Ni2p	C1s
As received	55	9	36
After photocatalysis	42	6	53
Oxidised at 500°C	62	38	-

It should be noted, that this is an average content of elements from depth of c.a. 1 nm with an assumption, that the elements are homogeneously distributed, which is not valid. Therefore these values should be taken as an approximation. The nickel foam oxidised at 500°C exhibit no carbon over the surface. The other nickel foams exhibit significant amount of carbon, which attenuates the Ni2p signal. This attenuation explains low values of Ni2p signals.

The deconvolution of C1s signal was performed on the basis of work [31]. The carbon species were observed on not oxidized nickel foam before and after photocatalytic process. The prominent shoulder on the left-hand side of the signal is related with carbon-oxygen species present over the surface of carbon. The intensity of C1s signal increased after the process i.e. the carbon coverage has increased. However both samples showed similar composition of an oxygen carbon species.

XPS spectra of Ni 2p signals indicated, that the highest intensity of Ni species had sample oxidised at 500°C. This can be attributed to absence of carbon over the surface of this sample. In case of other nickel foams the intensity of the Ni 2p signal was lower due to the carbon coverage, which attenuates the signal of Ni 2p. This signal can be deconvoluted to Ni^0, Ni^{2+}, Ni^{3+} (852.3, 853.8 and 855.8 eV, respectively [26]) and satellite signals. The signal of Ni^0 is negligible. The metallic Ni is present in the nickel foam, but the XPS sampling depth is c.a. 1 nm. Therefore the surface covered with oxides

 doi:10.20944/preprints202306.1825.v1

and carbon attenuates the signal from beneath. Nickel foam oxidized at 500°C showed clearly signals related to Ni^{2+} and Ni^{3+}, whereas, the other samples revealed mostly signal of Ni^{3+}.

The O1s can be unambiguously deconvoluted only for the sample oxidized at 500°C due to the absence of carbon. In case of other samples there are carbon-oxygen species, which contributes to O1s signal. This renders very difficult unambiguous deconvolution of the O1s spectrum. In case of the sample oxidised at 500°C two distinct components can be observed. One can be attributed to bulk nickel oxide and the other to the –OH groups present over the surface of nickel oxide. It is assumed, that a thin layer of Ni(oxy)hydroxide was formed on the surface of oxidized nickel foam.

4. Discussion

Nickel foam used as a support for TiO_2 showed spectacular properties for enhancement the photocatalytic decomposition of acetaldehyde under UV light irradiation. However, doping of the nanosized Ni particles to TiO_2 did not bring any advantages in either acetaldehyde decomposition nor mineralisation. Partly oxidized nickel foam also deteriorated the rate of acetaldehyde removal from a gas stream, although some other researchers indicated superiority of the oxidised nickel foam over that not oxidised [25]. These different properties of nickel materials could be explained by various reaction mechanisms occurred at the presence of TiO_2. Nanosized nickel after excitation can generate electrons, which can be transferred to the conductive band of TiO_2 or to the adsorbed species on its surface. From the other hand, the lifetime of these electrons is very short and they can undergo back transfer with heat generation. In case of oxidised Ni foam, there is also high probability of electron injection from the conductive band of NiO through the electron transfer zone – Ni (oxy)hydroxide to the TiO_2 due to the p-n heterojunction mechanism between these two semiconductors [32]. In such case, holes from the titania valence band can migrate to the lower energy valence band of NiO, decreasing possibility of hydroxyl radicals formation on TiO_2 surface, which are engaged in the mineralisation of organic compounds. Therefore very low mineralisation degree of acetaldehyde was observed for TiO_2 supported on the oxidised Ni foam. In case of not oxidised nickel foam, there is a low probability of electrons injection to the titania conductive band, due to the its other morphology, than the single Ni particles. There is a synergistic effect of combination TiO_2 with a nickel foam leading to the improved separation of charge carriers. Such phenomenon has been already described in the other research papers [28,33]. The other researchers proved an improvement of charge carriers separation through the detection of hydroxyl radicals and superoxide anion radicals under UV irradiation at the presence of nickel foam and Ni-MOF photocatalyst [28]. XPS measurements showed, that there is a thin layer of Ni (oxy)hydroxide formed on the surface of oxidised Ni foam. This layer can facilitate an interfacial electron transfer [34]. It is assumed, that the presence of this layer caused acceleration of electrons transfer from NiO to TiO_2. Not oxidised Ni foam exhibited some carbon species on the surface before and after photocatalytic process. Some impurities were observed on the surface of commercial Ni foam, which have disappeared after its use for the acetaldehyde decomposition. However XPS measurements indicated, that more carbonaceous species were present on the used Ni foam, than as receive. Some carbon deposits on Ni foam could be present due to the incomplete acetaldehyde decomposition. It is assumed, that these carbon species could act as an electron trap centres and contributed in the separation of charge carriers in TiO_2. In fact, process of acetaldehyde decomposition on the used Ni foam was much more efficient, than on the fresh one. Increase concentration of electrons on Ni foam facilitated adsorption of molecular oxygen and then superoxide anion radicals could be formed. Collecting of electrons on the surface of nickel foam could enhance mobility of holes in TiO_2 and can contribute in lag of e^-/h^+ pairs recombination. Holes take place in oxidation of acetaldehyde to acetic acid at the presence of air, according to the reaction:

$$h^+ + 3CH_3CHO + O_2 \rightarrow 2CH_3COOH + CH_3CO^\bullet + H^+ \quad (1)$$

The carbonyl radicals ($CH_3CO^\bullet$) are capable to react with O_2, which mediates the chain reactions of acetaldehyde oxidation, whereas formed acetic acid can undergo decomposition through the reaction with hydroxyl radicals [35]:

$$CH_3COOH + {}^\bullet OH \rightarrow CO_2 + H_2O + CH_3^\bullet \quad (2).$$

 doi:10.20944/preprints202306.1825.v1

Hydroxyl radicals can be formed by the reaction of holes with surface adsorbed hydroxyl ions:

$h^+ + {}^-OH \rightarrow {}^\bullet OH$ (3)

or in a double-electron oxygen reduction pathway [33]:

$O_2 + 2H^+ + 2e^- \rightarrow H_2O_2$ (4)

$H_2O_2 + e^- \rightarrow {}^\bullet OH + HO^-$ (5).

The other route od hydroxyl radicals formation can be through the single-electron reduction, conducted to formation superoxide anion radicals, which in further steps give yield in H_2O_2 production:

$e^- + O_2 \rightarrow O_2^{-\bullet}$ (6)

$O_2^{-\bullet} + H^+ \rightarrow HO_2^\bullet$ (7)

$2\ HO_2^\bullet \rightarrow H_2O_2 + O_2$ (8).

If the stored electrons in a nickel foam are engaged in formation of superoxide anion radicals or hydrogen peroxide species, then mineralisation of acetaldehyde is speeding up. As a consequence, formed on titania surface products of acetaldehyde conversion are faster removed, remaining the active sites free for new acetaldehyde molecules. In that way both, conversion and mineralisation of acetaldehyde are enhanced.

This process can be enhanced at the elevated temperature. It is assumed, that in the increased temperature higher quantity of H_2O_2 species are formed due to the increased mobility of electrons in the Ni conductive foam. Both, H_2O_2 species and formed upon its reduction hydroxyl radicals can take part in oxidation acetaldehyde and its conversion products. Therefore at the presence of Ni foam mineralisation degree of acetaldehyde was greatly enhanced.

The other researchers reported increased decomposition of acetaldehyde on TiO_2 doped with 0.5 % of Pt due to the spillover of oxygen from Pt to TiO_2 surface, which could oxidise byproducts of acetaldehyde conversion [17].

The other situation was noted in case of Au doped TiO_2, where, Au particles served as the active adsorption centres for acetaldehyde [36]. In that case Au nanoparticles oxidised acetaldehyde to acetic acid and then dissociated ions of acetate were transferred to TiO_2 surface, where underwent photochemical decomposition.

However, these studies showed, that doping of nanosized Ni species to TiO_2 did not enhanced its photocatalytic activity, even at elevated temperature. Possible direct transfer of electrons from dopant to TiO_2 could be detrimental for this process.

Mechanism of electron transfer between nickel material and TiO_2 was important to obtain an increased efficiency of acetaldehyde decomposition. In this case nickel foam with some adsorbed carbon oxygen species on its surface was suitable, because enhanced separation of free carriers and acetaldehyde mineralisation.

5. Conclusions

Performed studies on thermo-photocatalytic decomposition of acetaldehyde showed superior properties of nickel foam used as a support for TiO_2. It was evidenced, that nickel foam could improve photocatalytic properties of TiO_2 for acetaldehyde conversion at room temperature form 31 to 52% and at 100^{o}C from 40 to 85% with double increase of mineralisation degree. Even at lower temperature, such as 50^{o}C conversion of acetaldehyde on TiO_2 supported on nickel foam was high, because reached 80% (for TiO_2 itself maximal conversion of acetaldehyde was obtained at 75 ^{o}C with value of 46%). These results indicate on the synergistic effect between nickel foam and TiO_2, which can be utilised also in the other photocatalytic reactions, because charge separation in TiO_2 is a key factor, responsible for its photocatalytic activity. Using nickel foam as a support for TiO_2 gives high space for interaction of species between the interface boarder, therefore high enhancement of the photocatalytic yield was observed. Preparation of photocatalytic composites based on the nickel foam creates new direction of materials development.

Supplementary Materials: The following supporting information can be downloaded at: www.mdpi.com/xxx/s1, Figure S1: title; Table S1: title; Video S1: title.

Author Contributions: For research articles with several authors, a short paragraph specifying their individual contributions must be provided. The following statements should be used "Conceptualization, X.X. and Y.Y.; methodology, X.X.; software, X.X.; validation, X.X., Y.Y. and Z.Z.; formal analysis, X.X.; investigation, X.X.; resources, X.X.; data curation, X.X.; writing—original draft preparation, X.X.; writing—review and editing, X.X.; visualization, X.X.; supervision, X.X.; project administration, X.X.; funding acquisition, Y.Y. All authors have read and agreed to the published version of the manuscript." Please turn to the CRediT taxonomy for the term explanation. Authorship must be limited to those who have contributed substantially to the work reported.

Funding: This research was funded by the National Science Centre, Poland, grant nr 2020/39/B/ST8/01514.

Institutional Review Board Statement: In this section, you should add the Institutional Review Board Statement and approval number, if relevant to your study. You might choose to exclude this statement if the study did not require ethical approval. Please note that the Editorial Office might ask you for further information. Please add "The study was conducted in accordance with the Declaration of Helsinki, and approved by the Institutional Review Board (or Ethics Committee) of NAME OF INSTITUTE (protocol code XXX and date of approval)." for studies involving humans. OR "The animal study protocol was approved by the Institutional Review Board (or Ethics Committee) of NAME OF INSTITUTE (protocol code XXX and date of approval)." for studies involving animals. OR "Ethical review and approval were waived for this study due to REASON (please provide a detailed justification)." OR "Not applicable" for studies not involving humans or animals.

Informed Consent Statement: Any research article describing a study involving humans should contain this statement. Please add "Informed consent was obtained from all subjects involved in the study." OR "Patient consent was waived due to REASON (please provide a detailed justification)." OR "Not applicable." for studies not involving humans. You might also choose to exclude this statement if the study did not involve humans.

Written informed consent for publication must be obtained from participating patients who can be identified (including by the patients themselves). Please state "Written informed consent has been obtained from the patient(s) to publish this paper" if applicable.

Data Availability Statement: We encourage all authors of articles published in MDPI journals to share their research data. In this section, please provide details regarding where data supporting reported results can be found, including links to publicly archived datasets analyzed or generated during the study. Where no new data were created, or where data is unavailable due to privacy or ethical restrictions, a statement is still required. Suggested Data Availability Statements are available in section "MDPI Research Data Policies" at https://www.mdpi.com/ethics.

Acknowledgments: In this section, you can acknowledge any support given which is not covered by the author contribution or funding sections. This may include administrative and technical support, or donations in kind (e.g., materials used for experiments).

Conflicts of Interest: Declare conflicts of interest or state "The authors declare no conflict of interest." Authors must identify and declare any personal circumstances or interest that may be perceived as inappropriately influencing the representation or interpretation of reported research results. Any role of the funders in the design of the study; in the collection, analyses or interpretation of data; in the writing of the manuscript; or in the decision to publish the results must be declared in this section. If there is no role, please state "The funders had no role in the design of the study; in the collection, analyses, or interpretation of data; in the writing of the manuscript; or in the decision to publish the results".

References

1. Czelej, K.; Colmenares, J.C.; Jabłczyńska, K.; Ćwieka, K.; Werner, Ł.; Gradoń, L. Sustainable Hydrogen Production by Plasmonic Thermophotocatalysis. *Catalysis Today* **2021**, *380*, 156–186, doi:10.1016/j.cattod.2021.02.004.
2. Mateo, D.; Cerrillo, J.L.; Durini, S.; Gascon, J. Fundamentals and Applications of Photo-Thermal Catalysis. *Chem. Soc. Rev.* **2021**, *50*, 2173–2210, doi:10.1039/D0CS00357C.
3. Nair, V.; Muñoz-Batista, M.J.; Fernández-García, M.; Luque, R.; Colmenares, J.C. Thermo-Photocatalysis: Environmental and Energy Applications. *ChemSusChem* **2019**, *12*, 2098–2116, doi:10.1002/cssc.201900175.
4. Zhang, Y.; He, S.; Guo, W.; Hu, Y.; Huang, J.; Mulcahy, J.R.; Wei, W.D. Surface-Plasmon-Driven Hot Electron Photochemistry. *Chem. Rev.* **2018**, *118*, 2927–2954, doi:10.1021/acs.chemrev.7b00430.

5. Kumar, A.; Choudhary, P.; Kumar, A.; Camargo, P.H.C.; Krishnan, V. Recent Advances in Plasmonic Photocatalysis Based on TiO 2 and Noble Metal Nanoparticles for Energy Conversion, Environmental Remediation, and Organic Synthesis. *Small* **2022**, *18*, 2101638, doi:10.1002/smll.202101638.
6. Yao, C.; Zhang, L.; Wang, J.; He, Y.; Xin, J.; Wang, S.; Xu, H.; Zhang, Z. Gold Nanoparticle Mediated Phototherapy for Cancer. *Journal of Nanomaterials* **2016**, *2016*, 1–29, doi:10.1155/2016/5497136.
7. Adleman, J.R.; Boyd, D.A.; Goodwin, D.G.; Psaltis, D. Heterogenous Catalysis Mediated by Plasmon Heating. *Nano Lett.* **2009**, *9*, 4417–4423, doi:10.1021/nl902711n.
8. Yang, Q.; Xu, Q.; Yu, S.-H.; Jiang, H.-L. Pd Nanocubes@ZIF-8: Integration of Plasmon-Driven Photothermal Conversion with a Metal-Organic Framework for Efficient and Selective Catalysis. *Angew. Chem. Int. Ed.* **2016**, *55*, 3685–3689, doi:10.1002/anie.201510655.
9. Wang, F.; Huang, Y.; Chai, Z.; Zeng, M.; Li, Q.; Wang, Y.; Xu, D. Photothermal-Enhanced Catalysis in Core–Shell Plasmonic Hierarchical Cu 7 S 4 Microsphere@zeolitic Imidazole Framework-8. *Chem. Sci.* **2016**, *7*, 6887–6893, doi:10.1039/C6SC03239G.
10. Nikawa, T.; Naya, S.; Kimura, T.; Tada, H. Rapid Removal and Subsequent Low-Temperature Mineralization of Gaseous Acetaldehyde by the Dual Thermocatalysis of Gold Nanoparticle-Loaded Titanium(IV) Oxide. *Journal of Catalysis* **2015**, *326*, 9–14, doi:10.1016/j.jcat.2015.03.005.
11. Morikawa, T.; Ohwaki, T.; Suzuki, K.; Moribe, S.; Tero-Kubota, S. Visible-Light-Induced Photocatalytic Oxidation of Carboxylic Acids and Aldehydes over N-Doped TiO2 Loaded with Fe, Cu or Pt. *Applied Catalysis B: Environmental* **2008**, *83*, 56–62, doi:10.1016/j.apcatb.2008.01.034.
12. Liu, X.; Ye, L.; Ma, Z.; Han, C.; Wang, L.; Jia, Z.; Su, F.; Xie, H. Photothermal Effect of Infrared Light to Enhance Solar Catalytic Hydrogen Generation. *Catalysis Communications* **2017**, *102*, 13–16, doi:10.1016/j.catcom.2017.08.014.
13. Zhou, L.; Swearer, D.F.; Zhang, C.; Robatjazi, H.; Zhao, H.; Henderson, L.; Dong, L.; Christopher, P.; Carter, E.A.; Nordlander, P.; et al. Quantifying Hot Carrier and Thermal Contributions in Plasmonic Photocatalysis. *Science* **2018**, *362*, 69–72, doi:10.1126/science.aat6967.
14. Sarina, S.; Zhu, H.-Y.; Xiao, Q.; Jaatinen, E.; Jia, J.; Huang, Y.; Zheng, Z.; Wu, H. Viable Photocatalysts under Solar-Spectrum Irradiation: Nonplasmonic Metal Nanoparticles. *Angew. Chem. Int. Ed.* **2014**, *53*, 2935–2940, doi:10.1002/anie.201308145.
15. Hong, S.-J.; Mun, H.-J.; Kim, B.-J.; Kim, Y.-S. Characterization of Nickel Oxide Nanoparticles Synthesized under Low Temperature. *Micromachines* **2021**, *12*, 1168, doi:10.3390/mi12101168.
16. Kim, W.; Tachikawa, T.; Kim, H.; Lakshminarasimhan, N.; Murugan, P.; Park, H.; Majima, T.; Choi, W. Visible Light Photocatalytic Activities of Nitrogen and Platinum-Doped TiO2: Synergistic Effects of Co-Dopants. *Applied Catalysis B: Environmental* **2014**, *147*, 642–650, doi:10.1016/j.apcatb.2013.09.034.
17. Falconer, J.L.; Magrini-Bair, K.A. Photocatalytic and Thermal Catalytic Oxidation of Acetaldehyde on Pt/TiO2. *Journal of Catalysis* **1998**, *179*, 171–178, doi:10.1006/jcat.1998.2215.
18. Honda, M.; Ochiai, T.; Listiani, P.; Yamaguchi, Y.; Ichikawa, Y. Low-Temperature Synthesis of Cu-Doped Anatase TiO2 Nanostructures via Liquid Phase Deposition Method for Enhanced Photocatalysis. *Materials* **2023**, *16*, 639, doi:10.3390/ma16020639.
19. Sano, T.; Negishi, N.; Uchino, K.; Tanaka, J.; Matsuzawa, S.; Takeuchi, K. Photocatalytic Degradation of Gaseous Acetaldehyde on TiO2 with Photodeposited Metals and Metal Oxides. *Journal of Photochemistry and Photobiology A: Chemistry* **2003**, *160*, 93–98, doi:10.1016/S1010-6030(03)00226-0.
20. Zeng, Q.; Xie, X.; Wang, X.; Wang, Y.; Lu, G.; Pui, D.Y.H.; Sun, J. Enhanced Photocatalytic Performance of Ag@TiO2 for the Gaseous Acetaldehyde Photodegradation under Fluorescent Lamp. *Chemical Engineering Journal* **2018**, *341*, 83–92, doi:10.1016/j.cej.2018.02.015.
21. Zhu, S.; Xie, X.; Chen, S.-C.; Tong, S.; Lu, G.; Pui, D.Y.H.; Sun, J. Cu-Ni Nanowire-Based TiO 2 Hybrid for the Dynamic Photodegradation of Acetaldehyde Gas Pollutant under Visible Light. *Applied Surface Science* **2017**, *408*, 117–124, doi:10.1016/j.apsusc.2017.02.217.
22. Jiang, Y.; Chen, G.; Xu, X.; Chen, X.; Deng, S.; Smirnov, S.; Luo, H.; Zou, G. Direct Growth of Mesoporous Anatase TiO 2 on Nickel Foam by Soft Template Method as Binder-Free Anode for Lithium-Ion Batteries. *RSC Adv.* **2014**, *4*, 48938–48942, doi:10.1039/C4RA08395D.
23. Yan, Y.; Cheng, X.; Zhang, W.; Chen, G.; Li, H.; Konkin, A.; Sun, Z.; Sun, S.; Wang, D.; Schaaf, P. Plasma Hydrogenated TiO 2 /Nickel Foam as an Efficient Bifunctional Electrocatalyst for Overall Water Splitting. *ACS Sustainable Chem. Eng.* **2019**, *7*, 885–894, doi:10.1021/acssuschemeng.8b04496.
24. Zhang, Q.; Li, F.; Chang, X.; He, D. Comparison of Nickel Foam/Ag-Supported ZnO, TiO 2 , and WO 3 for Toluene Photodegradation. *Materials and Manufacturing Processes* **2014**, *29*, 789–794, doi:10.1080/10426914.2014.892616.
25. Hu, H.; Xiao, W.; Yuan, J.; Shi, J.; Chen, M.; Shang Guan, W. Preparations of TiO2 Film Coated on Foam Nickel Substrate by Sol-Gel Processes and Its Photocatalytic Activity for Degradation of Acetaldehyde. *Journal of Environmental Sciences* **2007**, *19*, 80–85, doi:10.1016/S1001-0742(07)60013-8.

26. Zeng, Q.; Chen, J.; Wan, Y.; Ni, J.; Ni, C.; Chen, H. Immobilizing TiO2 on Nickel Foam for an Enhanced Photocatalysis in NO Abatement under Visible Light. *J Mater Sci* **2022**, *57*, 15722–15736, doi:10.1007/s10853-022-07628-4.
27. Jia, J.; Li, D.; Cheng, X.; Wan, J.; Yu, X. Construction of Graphite/TiO 2 /Nickel Foam Photoelectrode and Its Enhanced Photocatalytic Activity. *Applied Catalysis A: General* **2016**, *525*, 128–136, doi:10.1016/j.apcata.2016.07.010.
28. Ding, X.; Liu, H.; Chen, J.; Wen, M.; Li, G.; An, T.; Zhao, H. *In Situ* Growth of Well-Aligned Ni-MOF Nanosheets on Nickel Foam for Enhanced Photocatalytic Degradation of Typical Volatile Organic Compounds. *Nanoscale* **2020**, *12*, 9462–9470, doi:10.1039/D0NR01027H.
29. Hu, H.; Xiao, W.; Yuan, J.; Shi, J.; He, D.; Shangguan, W. High Photocatalytic Activity and Stability for Decomposition of Gaseous Acetaldehyde on TiO2/Al2O3 Composite Films Coated on Foam Nickel Substrates by Sol-Gel Processes. *J Sol-Gel Sci Technol* **2008**, *45*, 1–8, doi:10.1007/s10971-007-1650-7.
30. Tryba, B.; Rychtowski, P.; Srenscek-Nazzal, J.; Przepiorski, J. The Inflence of TiO2 Structure on the Complete Decomposition of Acetaldehyde Gas. *Materials Research Bulletin* **2020**, *126*, 110816, doi:10.1016/j.materresbull.2020.110816.
31. Gęsikiewicz-Puchalska, A.; Zgrzebnicki, M.; Michalkiewicz, B.; Narkiewicz, U.; Morawski, A.W.; Wrobel, R.J. Improvement of CO 2 Uptake of Activated Carbons by Treatment with Mineral Acids. *Chemical Engineering Journal* **2017**, *309*, 159–171, doi:10.1016/j.cej.2016.10.005.
32. Zheng, D.; Zhao, H.; Wang, S.; Hu, J.; Chen, Z. NiO-TiO2 p-n Heterojunction for Solar Hydrogen Generation. *Catalysts* **2021**, *11*, 1427, doi:10.3390/catal11121427.
33. Xue, Y.; Shao, P.; Yuan, Y.; Shi, W.; Guo, Y.; Zhang, B.; Bao, X.; Cui, F. Monolithic Nickel Foam Supported Macro-Catalyst: Manipulation of Charge Transfer for Enhancement of Photo-Activity. *Chemical Engineering Journal* **2021**, *418*, 129456, doi:10.1016/j.cej.2021.129456.
34. Wan, K.; Luo, J.; Zhang, X.; Subramanian, P.; Fransaer, J. In-Situ Formation of Ni (Oxy)Hydroxide on Ni Foam as an Efficient Electrocatalyst for Oxygen Evolution Reaction. *International Journal of Hydrogen Energy* **2020**, *45*, 8490–8496, doi:10.1016/j.ijhydene.2020.01.043.
35. Pitchaimuthu, S.; Honda, K.; Suzuki, S.; Naito, A.; Suzuki, N.; Katsumata, K.; Nakata, K.; Ishida, N.; Kitamura, N.; Idemoto, Y.; et al. Solution Plasma Process-Derived Defect-Induced Heterophase Anatase/Brookite TiO 2 Nanocrystals for Enhanced Gaseous Photocatalytic Performance. *ACS Omega* **2018**, *3*, 898–905, doi:10.1021/acsomega.7b01698.
36. Nikawa, T.; Naya, S.; Tada, H. Rapid Removal and Decomposition of Gaseous Acetaldehyde by the Thermo- and Photo-Catalysis of Gold Nanoparticle-Loaded Anatase Titanium(IV) Oxide. *Journal of Colloid and Interface Science* **2015**, *456*, 161–165, doi:10.1016/j.jcis.2015.06.016.